

MD and Docking Studies Reveal That the Functional Switch of CYFIP1 is Mediated by a Butterfly-like Motion

Daniele Di Marino,^{†,‡,○} Giovanni Chillemi,[§] Silvia De Rubeis,^{†,‡,◆} Anna Tramontano,^{||,⊥,♯}
Tilmann Achsel,^{*,†,‡} and Claudia Bagni^{*,†,‡,▽}

[†]VIB Center for the Biology of Disease, KU Leuven, 3000 Leuven, Belgium

[‡]Center for Human Genetics, Leuven Research Institute for Neuroscience and Disease, KU Leuven, 3000 Leuven, Belgium

[§]SCAI SuperComputing Applications and Innovation Department, Cineca, Via dei Tizii 6, 00185 Rome, Italy

^{||}Department of Physics, Sapienza University of Rome, 00185 Rome, Italy

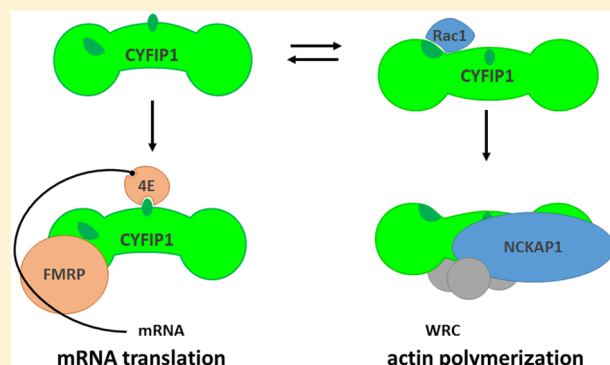
[⊥]Center for Life Nano Science @Sapienza, Istituto Italiano di Tecnologia, P.le Aldo Moro 5, 00185 Rome, Italy

[#]Istituto Pasteur, Fondazione Cenci Bolognetti, Sapienza University, P.le Aldo Moro 5, 00185 Rome, Italy

[▽]Department of Biomedicine and Prevention, University of Rome “Tor Vergata”, 00133 Rome, Italy

Supporting Information

ABSTRACT: Cytoplasmic FMRP interacting protein 1 (CYFIP1), also known as specifically RAC1 activated protein 1 (Sra1), plays a dual role: together with fragile X mental retardation protein (FMRP) and eIF4E it forms a complex that inhibits mRNA translation, while together with WAVE1, NCKAP1, ABI2, and HSPC300 it forms the WAVE regulatory complex (WRC) that upon RAC1 activation initiates actin polymerization. Here we performed a molecular dynamics (MD) simulation on CYFIP1 extracted from the known WRC structure, which shows that, in the absence of its WRC partners, a butterfly-like motion brings the two ends of CYFIP1 closer together, enabling the interaction with eIF4E. Our MD simulation is supported by available data showing that binding of CYFIP1 to eIF4E and binding to the WRC are mutually exclusive and that there is fluorescence resonance energy transfer between the N- and C-termini of CYFIP1. The differential interaction of RAC1–GTP with the two CYFIP1 structures predicts that RAC1 is directly responsible for the switch between these conformations.



INTRODUCTION

Fragile X syndrome is the most common form of inherited intellectual disability, affecting 1 in 4000 males and 1 in 8000 females.¹ Most cases are due to the transcriptional silencing of the *FMR1* gene as a consequence of a CGG expansion within its 5' untranslated region.^{1,2} The *FMR1* gene encodes the fragile X mental retardation protein (FMRP), an RNA-binding protein that represses the translation of associated mRNAs.^{3,4} A mechanism for FMRP-mediated translation regulation involves cytoplasmic FMRP interacting protein 1 (CYFIP1)⁵ and the translation initiation factor eIF4E.⁶ Similarly to general eIF4E-binding proteins (4E-BPs), CYFIP1 blocks access of eIF4G to eIF4E, thus inhibiting the assembly of the translation initiation machinery. Notably, CYFIP1 binds eIF4E through a non-canonical 4E-binding site (residues 724–732), which primarily implicates a lysine (Lys725) establishing an electrostatic interaction with a glutamate (Glu132) of eIF4E.⁶ Moreover, the CYFIP1–eIF4E inhibitory complex is tethered onto specific mRNAs through FMRP.⁶ In response to synaptic stimulation, the FMRP–CYFIP1 complex dissociates from eIF4E, and

translation of FMRP-repressed mRNAs ensues.⁶ This event requires activation of the small GTPase RAC1, which triggers the dissociation of CYFIP1–eIF4E.⁷

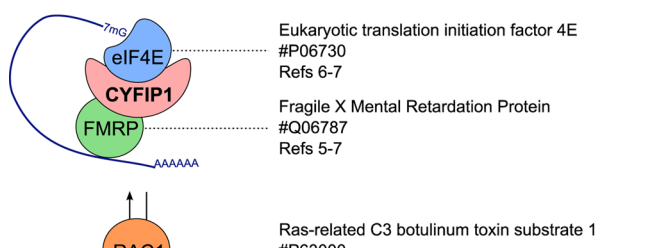
CYFIP1 is also part of the WAVE regulatory complex (WRC), a heteropentamer that controls actin rearrangements through the ARP2/3 complex.^{8–10} The structure of the WRC has been solved:¹⁰ CYFIP1 has a planar conformation and interacts with NCKAP1 via a large surface that accommodates the heterotrimer WAVE1:ABI2:HSPC300. CYFIP1 participates in the autoinhibition of the WRC by contributing to the surface that buries the verprolin homology, central and acidic region (VCA) motif of WAVE1,¹⁰ precluding activation of the ARP2/3 complex. The small GTPase RAC1 interacts with CYFIP1,^{11,12} and binding of active RAC1–GTP to CYFIP1 in a region adjacent to the inhibitory surface frees the VCA and thus activates ARP2/3.¹⁰ This event is supported, in a cooperative manner, by binding to phospholipids, by binding

Received: May 18, 2014

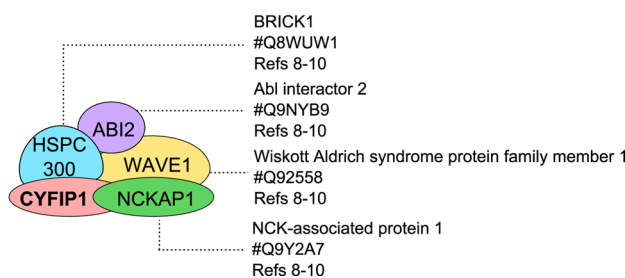
to a WIRS motif found in several membrane proteins, or by WAVE phosphorylation.^{13–16} In summary, CYFIP1 interacts with numerous proteins, serving as a platform for the assembly of two independent complexes (see Scheme 1 for a summary of the interactions relevant for this study).

Scheme 1. CYFIP1 Binding Partners^a

Translational complex



WAVE regulatory complex (WRC)



^aThe acronyms of the proteins that directly bind CYFIP1 are listed together with their full names, Uniprot IDs, and corresponding references. The protein partners are sorted according to the two CYFIP1 complexes; RAC1 regulates both complexes but is not assigned to either of them.

Importantly, on the basis of the published structure of the WRC, the planar conformation of CYFIP1 does not allow easy access to the eIF4E-binding region.^{7,10} CYFIP1 can associate with only one complex at a time, either the WRC or the translation-inhibiting complex, thus creating a homeostasis between the two complexes.⁷ A preliminary molecular dynamics (MD) simulation of CYFIP1 free in solution led us to hypothesize that CYFIP1 exists in two conformations (which was experimentally confirmed) and that a conformational switch in CYFIP1 allows access by either eIF4E or the WRC components and therefore dictates its partitioning between the two complexes.⁷

While our preliminary simulation provided only a snapshot of the two CYFIP1 conformations, in the present work we studied the dynamic evolution of the conformational change in order to understand its structural consequences for the interactions with key binding partners. We used extensive MD simulations (135 ns) to study the conformational changes in CYFIP1 at the molecular level, following the free protein and the NCKAP1 complex. We show that free CYFIP1 undergoes a butterfly-like motion that bends the N- and C-terminal domains toward the central one, resulting in a more globular conformation. Conversely, when bound to NCKAP1, CYFIP1

maintains a planar conformation. The conformational change reorients helix H8b, part of the eIF4E binding site, rendering it more accessible for eIF4E. No similar motion was observed in the simulation of the CYFIP1–NCKAP1 dimer. Accordingly, docking experiments indicated an increased affinity of CYFIP1 for eIF4E in the globular conformation with respect to the conformation in the dimer. Importantly, our docking analysis shows that the globular conformation has a steeply decreased affinity for RAC1–GTP and suggests how RAC1 can shift CYFIP1 from one complex to the other. These findings provide a detailed structural explanation for the dual role of CYFIP1.

METHODS

Molecular Dynamics Simulation. Initial coordinates for CYFIP1 and the CYFIP1–NCKAP1 heterodimer were obtained from the X-ray structure of the WRC (PDB ID 3P8C). This includes CYFIP1, NCKAP1, WAVE1, Abi2, and HSPC300. The residue numbering is the same as in the X-ray structure.¹⁰ Here the CYFIP1 structure defined in the crystal is denoted as CYFIP1_{XRAY}. The structure of the CYFIP1–NCKAP1 heterodimer was considered for the simulation instead of the whole WRC. This was done for two reasons: first, the structures of the WAVE1, Abi2, and HSPC300 proteins have been only partially resolved, and the lacking portions are too big to be modeled; second, but more importantly, the heterodimer represents the base scaffold for the assembly of the WRC complex, so it well represents the properties of CYFIP1 in the WRC. The N-terminal helix of CYFIP1 is connected to the rest of the structure through a flexible loop (residues 23–56) that was not resolved in the X-ray structure because of its high degree of fluctuation; for this reason, residues 1–56 were not included in our model. The starting positions of four unstructured loops in the N-terminal domain (residues 338–344, 368–379, 540–542, and 572–577) and one in the C-terminal domain (residues 1228–1236) were obtained by using the loop database in Swiss PDB Viewer version 5.7¹⁷ and further regularized with the Powell minimization algorithm implemented in the Sybyl package.¹⁸

The MD simulation was performed with NAMD 2.8 package for GPU computing¹⁹ using the CHARMM c31b1 force field.^{20,21} CYFIP1 was immersed in a rectangular simulative box filled with 176688 TIP3P explicit solvent molecules and rendered electroneutral by the introduction of two sodium counterions (final system of 549575 explicit atoms). Similarly, the CYFIP1–NCKAP1 dimer was immersed in a rectangular box solvated with 179411 water molecules and neutralized by the addition of 19 sodium counterions (final system of 575698 explicit atoms).

The following simulation protocol was applied to both systems. The lengths of all of the hydrogen bonds were constrained by applying the LINCS algorithm,²² and electrostatic interactions were taken into account by the particle mesh Ewald method^{23,24} using a cutoff of 1.2 nm for the evaluation of short-range nonbonded interactions. A first round of minimization using the steepest descent algorithm was performed for 10000 steps in order to regularize the structures. Optimization and relaxation of solvent and ions were performed by simulating the system at temperatures of 50, 100, 150, 200, and 250 K for 500 ps each with a time step of 1.0 fs. CYFIP1 and the CYFIP1–NCKAP1 dimer were then subjected to an MD simulation for 135 ns. The simulation was carried out with a time step of 2.0 fs at a constant temperature

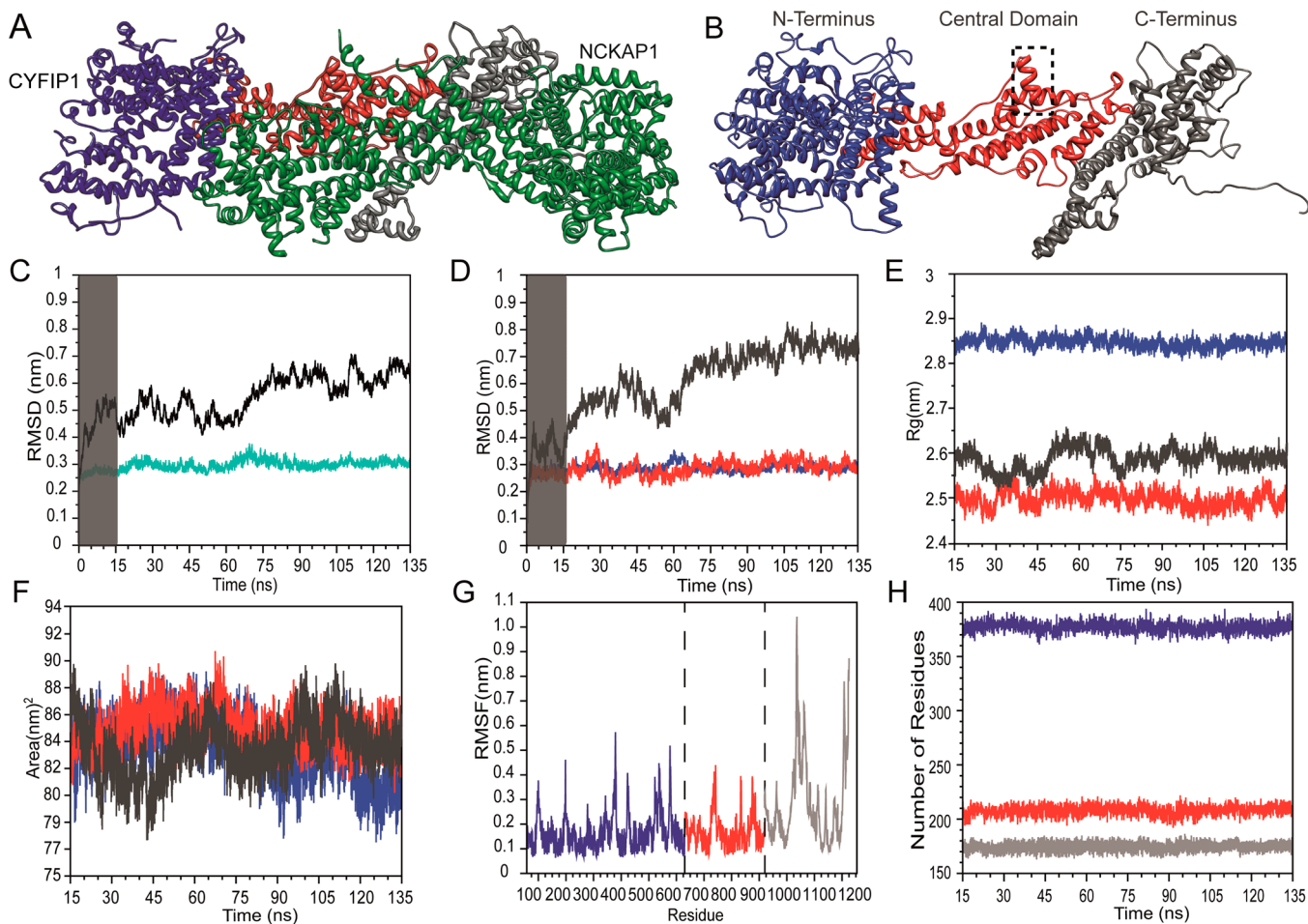


Figure 1. Domain structure and conformational evolution of CYFIP1. (A) Ribbon representation of the CYFIP1–NCKAP1 heterodimer solved by Chen et al.¹⁰ The structure of CYFIP1 is divided into N-terminal (blue), central (red), and C-terminal (gray) domains. NCKAP1 is shown in green. (B) Ribbon representation of the three CYFIP1 domains (N-terminal, central, and C-terminal) shown in blue, red, and gray, respectively. The structure was extracted from that of the heterodimer solved by Chen et al.¹⁰ Helix H8b in the central domain, containing the eIF4E-binding site, is highlighted by a dashed rectangle. (C) Plot of the root-mean-square deviations (RMSDs) calculated for free CYFIP1 (black line) and CYFIP1 bound to NCKAP1 (cyan line) as functions of simulation time. The first 15 ns (shaded) is considered equilibration/thermalization time. (D) Plot of the RMSDs (calculated using the average of all structures as a reference) of the N-terminal (blue), central (red), and C-terminal (gray) domains of CYFIP1 free in solution as functions of time. (E) Plot of the radii of gyration (R_g) as in (D). The thermalization phase has been omitted in this graph. (F) Plot of solvent-accessible surface area (SASA) as in (E). The thermalization phase has been omitted. (G) Root-mean-square fluctuation (RMSF) for each residue. The residue number is given on the x axis, and the domains are color-coded as before. (H) Time evolution of the numbers of residues in α -helices for each of the three domains composing CYFIP1 (as in D). The thermalization phase has been omitted.

of 300 K using the Langevin method⁴¹ and a constant pressure of 1 bar using the Nosé–Hoover algorithm.^{26,27}

In order to check the reproducibility of the results, the simulation of free CYFIP1 was carried out four times. These replicas were generated by reassigning the atomic velocities to four configurations taken at 200 ps (replica R1), 1.7 ns (R2), 3.7 ns (R3), and 5.0 ns (R4), respectively, in accordance with the required Maxwell–Boltzmann distribution. Each replica was carried out until a final time of 30 ns.

Molecular Dynamics Analyses. Analyses of the simulations of both systems were carried out on the last 120 ns of the simulations, as the first 15 ns was considered as equilibration time. Root-mean-square deviations (RMSDs), root-mean-square fluctuations (RMSFs), solvent-accessible surface areas (SASAs), salt bridges, principal component analyses (PCAs), and structural clustering were obtained using the GROMACS 4.5.3 package.²⁸ The images were obtained with the PyMOL molecular graphics system, version

1.2r2²⁹ and UCSF Chimera,³⁰ and the graphs were obtained with xmGrace (<http://plasma-gate.weizmann.ac.il/Grace/>).

The distance between the N-terminus and the C-terminus was measured by considering the centers of masses of the following two groups: in the N terminus, residues 2–5, 73–86, and 445–454; in the C terminus, residues 902–917 and 1129–1154.

PCA was carried out on the 1194 $\text{C}\alpha$ atoms of the protein and on 24000 frames (i.e., one frame every 5 ps of simulation time).^{31,32} The method, based on diagonalization of the covariance matrix built from the atomic fluctuations after the removal of the translational and rotational movements, allows the identification of the $3N$ directions along which the majority of the protein correlated motions are defined.

The CYFIP1 conformations were clustered with the g_cluster program in GROMACS 4.5.3²⁸ using the Gromos algorithm.³³ The clustering was performed on 12000 structures (i.e., one every 10 ps of simulation time).

The structure with the largest number of neighbors (i.e., configurations within the cutoff range) was taken as the centroid of the first cluster and eliminated from the pool with all of its neighbors. The process was repeated until all of the structures were assigned to a cluster. The number of clusters depends on the adopted threshold value; to obtain a maximum number of eight clusters, a threshold value of 0.3 nm was used. The centroid structure of the most populated cluster is denoted as CYFIP1_{MD} and was used for molecular docking. The structure of eIF4E was taken from the ternary eIF4E/m7GpppA/4E-BP1 complex (PBD ID 1WKW).³⁴

Molecular Docking. Docking of eIF4E with CYFIP1_{XRAY} and CYFIP1_{MD} was performed using the HADDOCK program in rigid-body mode. On the basis of previous docking simulations and experimental data,⁶ the residues Asp724–Lys732 in CYFIP1 and Trp73 and Glu132 in eIF4E were defined as “active residues” in HADDOCK.

Each docking experiment consisted of 200 runs. The complexes with the best HADDOCK scores belonging to the most populated cluster were analyzed to detect the changes in CYFIP1–eIF4E affinity during the MD simulation. Finally, the CYFIP1_{MD}–eIF4E and CYFIP1_{XRAY}–eIF4E electrostatic interactions were calculated using the Protein Interactions Calculator Web server³⁵ with a distance cutoff of 0.6 nm.

■ RESULTS

CYFIP1 is Organized into Three Domains with Distinct Properties.

The WRC crystal structure¹⁰ revealed that CYFIP1 has a planar conformation when it interacts with the WRC (Figure 1A). To study whether and how the CYFIP1 structure changes when released from WRC, we carried out an MD simulation of CYFIP1 free in solution for 135 ns (Figure 1B). A second simulation was performed on the CYFIP1–NCKAP1 dimer, which represents the scaffold for the assembly of the WRC complex. From here on, the structure of CYFIP1 extracted from the WRC¹⁰ will be denoted as CYFIP1_{XRAY}, while the structure generated by MD will be denoted as CYFIP1_{MD}.

The structure of CYFIP1 is divided into three domains (Figure 1B): the N-terminal domain (residues 57–632, shown in blue), the central domain (residues 633–921, shown in red), and the C-terminal domain (residues 922–1250, shown in dark gray). The N-terminal domain is the largest and is characterized by a compact globular shape mainly composed of α -helices; it contains most of the binding site for RAC1.¹⁰ The central domain has a planar shape and includes several α -helices with different lengths; helix H8b (residues 724–732, indicated by the dashed box in Figure 1B) is involved in the binding to eIF4E.⁶ Notably, the region surrounding helix H8b is not solvent accessible: it is covered on one side by other CYFIP1 domains and on the other by the N-terminal helix of NCKAP1¹⁰ (compare boxed region in Figure 1B with the corresponding region in Figure 1A). The C-terminal domain also has a globular shape and, together with the central domain, is involved in the interaction with NCKAP1 (Figure 1A,B).

During the 135 ns simulation, CYFIP1 free in solution moved away from the starting X-ray structure, reaching a final $\text{C}\alpha$ RMSD of 0.7 nm (Figure 1C, black line). In contrast, the CYFIP1–NCKAP1 dimer simulation did not show a deviation from the initial structure; the RMSD remained stable at around 0.28 nm during the stimulation (Figure 1C, cyan line).

The observed RMSDs of CYFIP1 were mainly due to movements in its C-terminal domain (Figure 1D, gray line)

while the N-terminal and central domains did not substantially deviate from the conformations observed in CYFIP1_{XRAY} (Figure 1D, blue and red lines, respectively). The larger structural flexibility of the C-terminal domain is likely caused by the absence of its binding partner, NCKAP1. Further support that the C-terminal domain is mainly responsible for the structural arrangements described above came from measuring the radii of gyration (R_g), SASAs, RMSFs, and α -helical contents, which were calculated after eliminating the last 24 residues that represent an unstructured tail of the domain (Figure 1E–H). The radius of gyration calculated as a function of simulation time for CYFIP1_{MD} shows that the protein is reorganizing its conformation, as demonstrated by the drop in the value from ~5.2 nm to ~4.9 nm (Figure S1C in the Supporting Information). The values of R_g for CYFIP1_{MD} separately calculated for the N-terminal and central domains have rather constant values of 2.85 and 2.5 nm, respectively, along the entire trajectory (Figure 1E, blue and red, respectively). Conversely R_g of the C-terminal domain is highly variable at the beginning of the simulation, ranging between 2.5 and 2.65 nm during the first 80 ns before stabilizing (Figure 1E, gray), which indicates that CYFIP1 has spontaneously moved away from the starting X-ray conformational basin toward an energetically more favorable one. On the other hand, the R_g values for CYFIP1 and NCKAP1 in the WRC are fairly constant during the entire simulation (Figure S1D in the Supporting Information).

The three domains all undergo changes in their solvent-accessible surface areas (Figure 1F). The N- and C-terminal domains showed larger variations in their SASAs (average values 117 ± 2.1 and $69 \pm 2.0 \text{ nm}^2$, respectively), while the SASA of the central domain remained more stable during the simulation (average $70 \pm 1.2 \text{ nm}^2$). The RMSF values (Figure 1G) showed that the C-terminal domain fluctuated more than the others during the simulation; in particular, the region between residues 1025 and 1075 fluctuated up to 1.1 nm. The high profile of fluctuation of this region is due to its particular structure. Indeed, it is composed of four alpha helices, three short and one long, that protrude out of the compact structure of the C-terminal domain directly into the solvent. This 100 amino acid region is a kind of “arm” that could be responsible for the interaction with other molecular partners of CYFIP1. The central domain was much more stable, with the great majority of residues fluctuating less than 0.2 nm. It is worth mentioning that its most mobile region, around residues 720–750, includes the short helix H8b involved in the interaction with eIF4E. The fluctuations of the molecule observed during the simulation do not involve changes in the stability of the secondary structure elements. Indeed, the number of residues in α -helices for each CYFIP1 domain remains rather constant throughout the simulation (Figure 1H). When the same analyses were performed on the CYFIP1–NCKAP1 complex, no relevant structural fluctuations were observed (Figure S1E in the Supporting Information).

Altogether, these analyses suggest that when CYFIP1 is not engaged with the WRC, it undergoes structural rearrangements, most of which involve its C-terminal domain.

A Butterfly-like Motion Underlies the CYFIP1 Conformational Changes. We next studied the motions of CYFIP1 during the simulation by principal component analysis (PCA), which allows discrimination of the concerted motions of a protein (often related to biological functions) from uncorrelated fluctuations. The result of a PCA is a list of

eigenvectors, each describing a part of the analyzed data set defining direction and component of the motion. In our case, the motions along the first three eigenvectors explain 64% of the total motion (34% for the first, 18% for the second, and 12% for the third component; Figure 2A). This analysis reveals

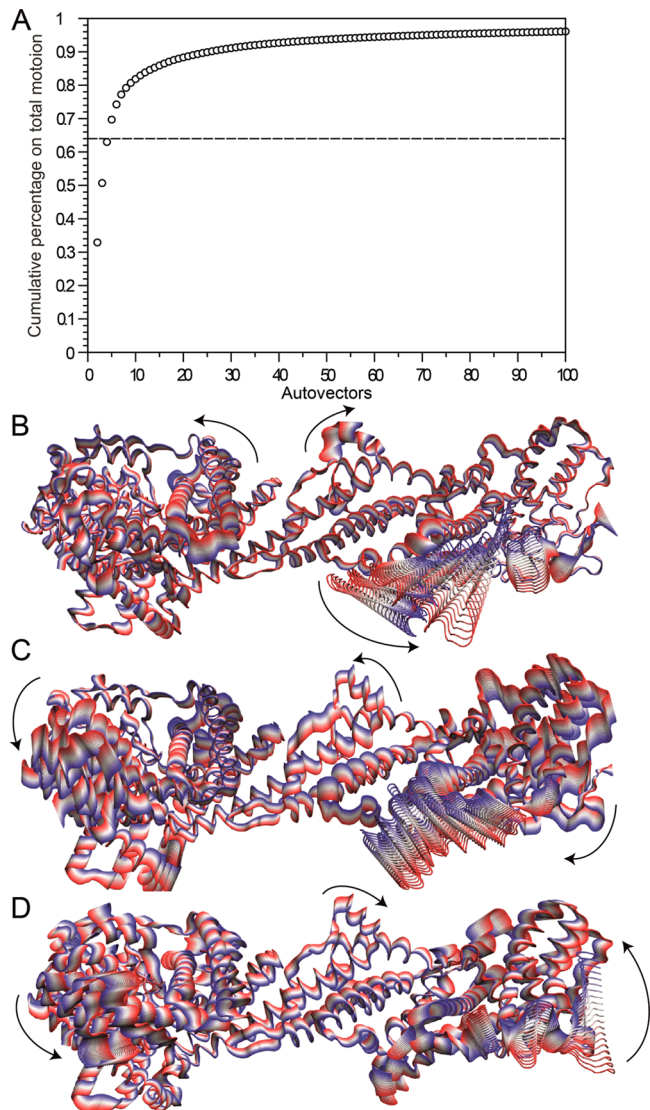


Figure 2. Analysis of the principal components of the motion in CYFIP1_{MD}. (A) Cumulative percentage of the eigenvalues in the principal component analysis. Eigenvectors with smaller eigenvalues describe less correlated protein fluctuations. (B–D) Projections of the atomic trajectories over the first, second, and third eigenvectors, respectively. Twenty frames per projection are shown, from the average structure (white) to the highest positive (red) and negative (blue) eigenvalues with the color code red–white–blue following the trajectory evolution time.

concerted long-range rearrangements of the CYFIP1 domains. The projection of the MD trajectory along the first eigenvector captures a motion that reflects coordinated bending of the terminal domains over the central domain in a butterfly-like fashion. Notably, during this movement, helix H8b reorients by rotating and translating with respect to the remaining portion of the central domain (Figure 2B; also see the movie in the Supporting Information). The second and third eigenvectors represent a torsion of the terminal domains against each other

and an anticorrelated motion of the terminal domains with respect to the central domain, respectively (Figure 2C,D). These data indicate that the three CYFIP1 domains undergo long-range correlated motions, orchestrating a butterfly-like motion.

As a result of this motion, the distance between the N- and C-termini (Figure 3) varied substantially, ranging from 12 nm

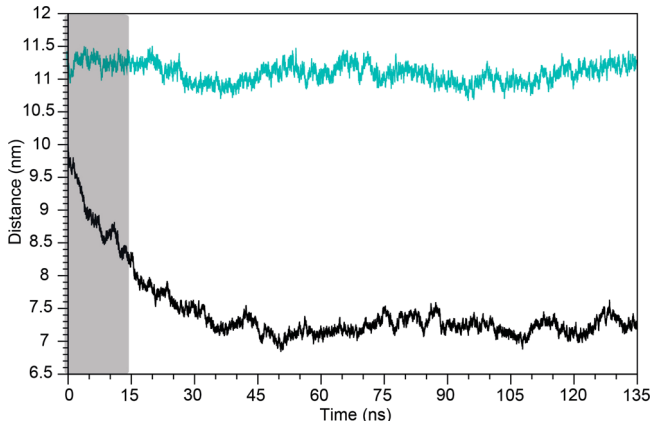


Figure 3. The terminal domains of CYFIP1 move closer to each other during simulation. Shown is a plot of the distances between the centers of mass of the terminal extremities for CYFIP1 (black line) and CYFIP1–NCKAP1 (cyan line) as functions of the simulation time. The gray bar represents the equilibration time, which was discarded from the other MD analyses.

in CYFIP1_{XRAY} to ~10 nm during the first 2.5 ns of the simulation (i.e., the thermalization phase) and reaching a plateau at ~7 nm after 50 ns of simulation (CYFIP1 free, black line). This movement of the terminal domains toward each other is reproducible: four replica simulations starting at different coordinates arrive at similar distances between the N- and C termini (Figure S2 in the Supporting Information). As expected, the equivalent distance in CYFIP1 in the NCKAP1 complex was more constant, reaching ~11.5 nm during the thermalization phase and then remaining essentially constant during the simulation (Figure 3, light-blue line). PCA performed on CYFIP1 in complex with NCKAP1 shows that the first three eigenvectors represent in this case ~40% of the total motion (Figure S3A in the Supporting Information). The motion described by these eigenvectors is very restricted, and there is no change in the orientation between the different domains (Figure S3B–D in the Supporting Information).

In summary, these results suggest that CYFIP1 might exist in a conformation alternative to the one described in the WRC crystal (CYFIP1_{XRAY}), which we call here CYFIP1_{MD}. The latter conformation is more globular and compact and, as we will show in the following, more suitable for binding of eIF4E.

The CYFIP1 Conformational Rearrangement Promotes the Interaction with eIF4E. We hypothesized that the rearrangement observed in CYFIP1_{MD} with the described butterfly-like motion, might promote the binding of CYFIP1 to eIF4E. Essentially, this binding occurs thanks to the presence of a short helix (H8b) localized in the central domain of CYFIP1⁶ that creates a network of interactions with a specific convex surface of eIF4E.⁶ Consequently, we analyzed in detail the interactions of helix H8b, which contains the eIF4E-binding site. The helix is characterized by an alternation of positively and negatively charged amino acids¹⁰ (Figure 4A). The

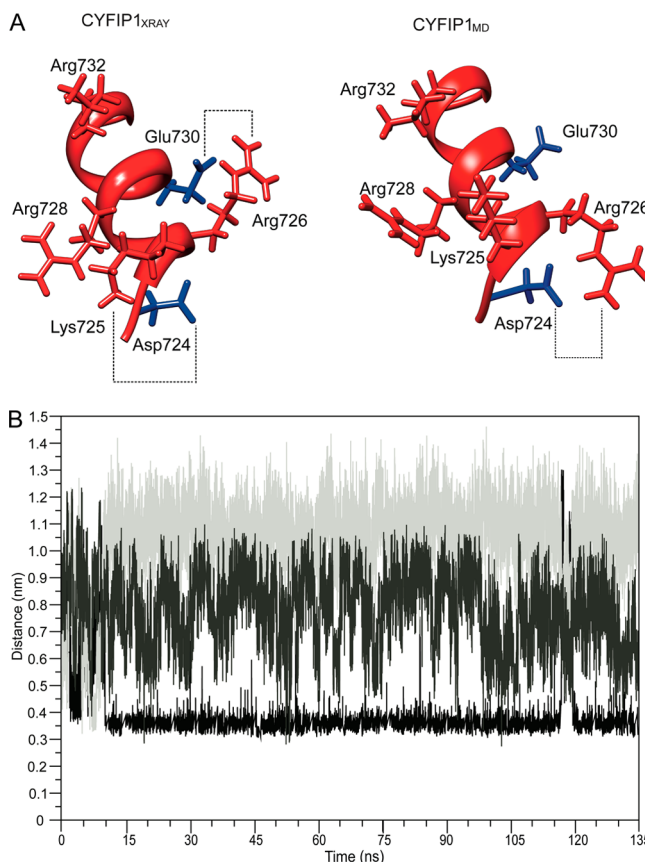


Figure 4. Electrostatic features of CYFIP1 helix H8b, which is involved in the interaction with eIF4E. (A) Structures of helix H8b in the central domain from (left) CYFIP1_{XRAY} and (right) CYFIP1_{MD}. Positively and negatively charged residues are shown in red and blue. Dotted lines indicate potential salt bridges between Asp724 and Lys725, Asp724 and Arg726, and Arg726 and Glu730. (B) Distances between charged atoms for the three potential salt bridge pairs Asp724–Lys725 (light gray), Arg726–Glu730 (dark gray), and Asp724–Arg726 (black). Only the Asp724–Arg726 pair forms a salt bridge for nearly the whole simulation time.

distances between the potential salt bridge pairs Asp724–Lys725, Asp724–Arg726, and Arg726–Glu730 drastically changed during the simulation: In CYFIP1_{XRAY}, Arg726 forms a salt bridge with Glu730 (with a distance of 0.45 nm between the side chains), while Asp724 engages neither Lys725 nor Arg726 (with a distance of 0.8 nm for both pairs) (Figure 4A, CYFIP1_{XRAY}). Already during the thermalization phase (the first 15 ns of the simulation), a salt bridge forms between Asp724 and Arg726, and it remains rather stable at a distance of ~0.35 nm throughout the rest of the simulation (Figure 4A, CYFIP1_{MD}, and Figure 4B, black line). This salt bridge fixes Lys725 in a position pointing away from the helix (the distance to Asp724 is >1.0 nm for most of the simulation; Figure 4A, CYFIP1_{MD}, and Figure 4B, light-gray line), in agreement with the modeling of the isolated eIF4E-binding peptide.⁶ The salt bridge Arg726–Glu730 finally was destabilized, and the distance between the two partners fluctuated widely (average of 0.78 nm; Figure 4A, CYFIP1_{MD}, and Figure 4B dark-gray line). In summary, the rearrangements orient Lys725, which is crucial for eIF4E binding,⁶ into a position where it can best interact with Glu132 of eIF4E.

To verify whether these structural changes might affect the CYFIP1–eIF4E interaction, we performed docking experi-

ments to study the interaction between eIF4E^{34,36} and CYFIP1_{XRAY}¹⁰ or CYFIP1_{MD}. We first clustered the conformations explored by CYFIP1_{MD} after thermalization (first 15 ns) according to the RMSDs among their C_α atoms. This led to the definition of eight families of structures, four of which included more than 1000 structures out of the total of 12000 (Figure 5A,B). Among these families, the most populated includes 6000 structures (Figure 5B), all of which were sampled between 60 and 135 ns (Figure 5A). Comparison to Figure 3 demonstrates that this most populated cluster is representative of CYFIP1 in its globular conformation (i.e., the distance between the centers of mass of the terminal domains is at a minimum). In the following, we carried out a docking analysis of eIF4E onto the crystallographic structure (CYFIP1_{XRAY}) and the centroid of the most populated cluster (CYFIP1_{MD}). The plot of the distance between the N- and C-termini versus the projection along the second eigenvector was calculated in order to detect whether the structure selected for the docking is representative of a well-sampled family of conformations. Indeed, the graph (reported in Figure S4 in the Supporting Information) shows that the selected CYFIP1_{MD} structure lies in the middle of a well-populated region, indicating that this conformation is energetically favorable.

The predicted CYFIP1_{XRAY}–eIF4E complex with the lowest HADDOCK score (−38) is stabilized by only two salt bridges, excluding the Lys725–Glu132 pairing that was experimentally shown to be crucial for eIF4E–CYFIP1 binding,⁶ since the two residues are at a distance of 1.9 nm from each other (Figure 5C). Conversely, CYFIP1_{MD}–eIF4E docking reaches a better HADDOCK score (−48 in the best complex). In this complex, CYFIP1–Lys725 and eIF4E–Glu132 are close enough to form a salt bridge (0.4 nm), allowing better access of eIF4E to the central domain (Figure 5D). In total, the CYFIP1_{MD}–eIF4E complex is stabilized by five salt bridges (Table 1). Our data therefore show that the change of CYFIP1 from the planar conformation to a more globular conformation allows a “structure-specific” recognition by eIF4E.

To corroborate the evidence that CYFIP1_{MD} is more prone to interact with eIF4E, we compared the eIF4E/4E-BP crystal structure³⁴ with the modeled CYFIP1_{XRAY}–eIF4E and CYFIP1_{MD}–eIF4E complexes. The helix engaging eIF4E–Glu132 is oriented very similarly in the CYFIP1_{MD}–eIF4E and the eIF4E/4E-BP complex, while the same helix is positioned differently in the CYFIP1_{XRAY}–eIF4E complex (Figure S5 in the Supporting Information). It can thus be concluded that during the MD simulation CYFIP1 evolved into a more globular conformation with increased affinity for eIF4E.

The New CYFIP1 Conformation Is Less Suitable for the Interaction with RAC1. RAC1–GTP activates the WRC because its binding to CYFIP1 induces the release of the VCA domain.^{14,16} In addition, active RAC1–GTP promotes the shift of CYFIP1 from the eIF4E complex into the WRC.⁷ To see whether RAC1–GTP could differentially interact with the two complexes, we simulated docking of the RAC1–GTP structure³⁷ to the two CYFIP1 conformations. RAC1–GTP docks well to the planar CYFIP1_{XRAY} conformation, involving numerous residues belonging to four regions of RAC1 (Table 2) and thus obtaining a favorable HADDOCK score of −77. Notably, the five CYFIP1 residues that were experimentally shown to be involved in RAC1 binding¹⁰ are all part of the binding surface determined by our simulation (Cys179, Arg190, Glu434, Phe626, and Met632; see the detailed view in Figure 6A). In agreement with experimental data,¹⁰ our model also

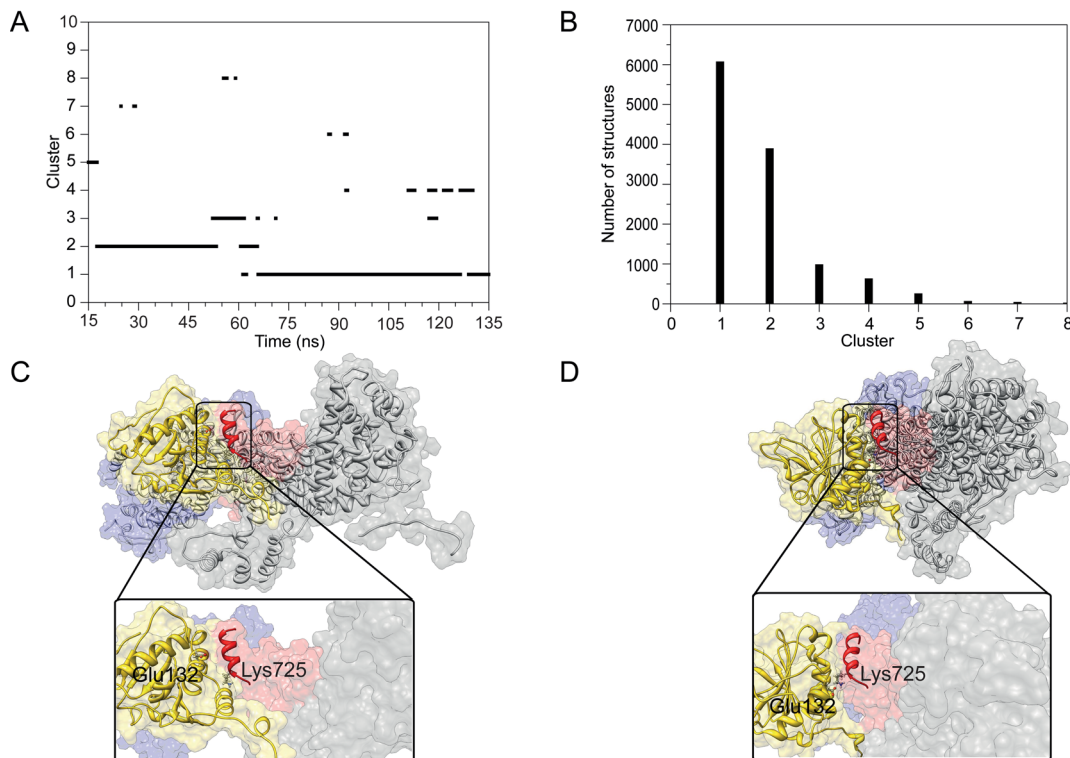


Figure 5. CYFIP1 helix H8b orientation and interaction with eIF4E, as characterized by cluster and docking analysis. (A) Time evolution of the simulation structures assigned to each cluster. (B) Number of simulation structures assigned to each cluster. (C, D) Analyses of the docking of eIF4E with (C) CYFIP1_{XRAY} and (D) CYFIP1 in the globular conformation sampled by MD, represented by the centroid of the most populous cluster. In the latter docking, the orientation of helix H8b allows an energetically favorable interaction of Lys725 with Glu132. The insets show details of the interfaces between CYFIP1 and eIF4E.

Table 1. Five Salt Bridges That Stabilize the Complex of eIF4E with Globular CYFIP1_{MD}^a

eIF4E	interacting with	
	CYFIP1 _{XRAY}	CYFIP1 _{MD}
Glu32	—	Arg832
Asp127	Lys750	Lys732
Arg128	—	Asp724
Glu132	Arg744	Lys725
		Arg728

^aSalt bridge interactions in the CYFIP1–eIF4E complex after docking calculations using the crystallographic structure (CYFIP1_{XRAY}) and the simulated structure (CYFIP1_{MD}). A salt bridge was scored when the two residues were of opposite electric charge and located at a distance of less than 0.6 nm. The functionally important salt bridge Glu132–Lys725 is highlighted in bold.

Table 2. Definition of the RAC1 Regions Interacting with CYFIP1_{XRAY}^a

	RAC1 region	CYFIP1 domain
region I	Val48, Asp49, Gly50	N-terminal
region II	Asp123, Lys125, Ile128, Asp129, Lys132, Asp133	central
region III	Pro141, Leu145, Lys149	N-terminal
region IV	Arg165, Thr169, Asp172, Arg176	N-terminal

^aListed are the four regions of RAC1 that interact with CYFIP1_{XRAY} in our docking calculations, the respective amino acids that contribute most to the interactions, and the CYFIP1 domains with which they interact.

predicts that WAVE1 increases the strength of CYFIP1–RAC1 binding by contributing to the interaction surface (Figure S6A in the Supporting Information). When the same docking parameters were used on the globular CYFIP1_{MD} structure (see Methods), RAC1–GTP was found to bind only to the N-terminus of CYFIP1, leaving the experimentally verified RAC1-binding residues free (see the detailed view in Figure 6B), preventing an interaction of RAC1 with WAVE1 (Figure S6B in the Supporting Information) and giving a rather unfavorable HADDOCK score of 50. Thus, we predict that RAC1–GTP binds only to the CYFIP1_{XRAY} conformation and therefore could well play an active role in the conformational rearrangement (see the Discussion).

DISCUSSION

There are many examples of “moonlighting” proteins that perform more than one function depending on their structural conformation and/or subcellular localization.³⁸ CYFIP1 has two roles: it represses the synthesis of specific proteins and regulates actin polymerization. The coordination of these two processes occurs through the shift of CYFIP1 from the eIF4E complex to the WRC, which is induced by active RAC1⁷ (Scheme 1). Since both functions take place in the same subcellular compartment, e.g., the neuronal synapse, a conformational switch in CYFIP1 seems likely to determine which role CYFIP1 is playing at a given moment.

In this study, we were able to simulate the evolution of the known CYFIP1 structure, a 145 kDa protein, using molecular dynamics. We have shown that CYFIP1 is able to undergo a butterfly-like motion, switching from the planar structure of the

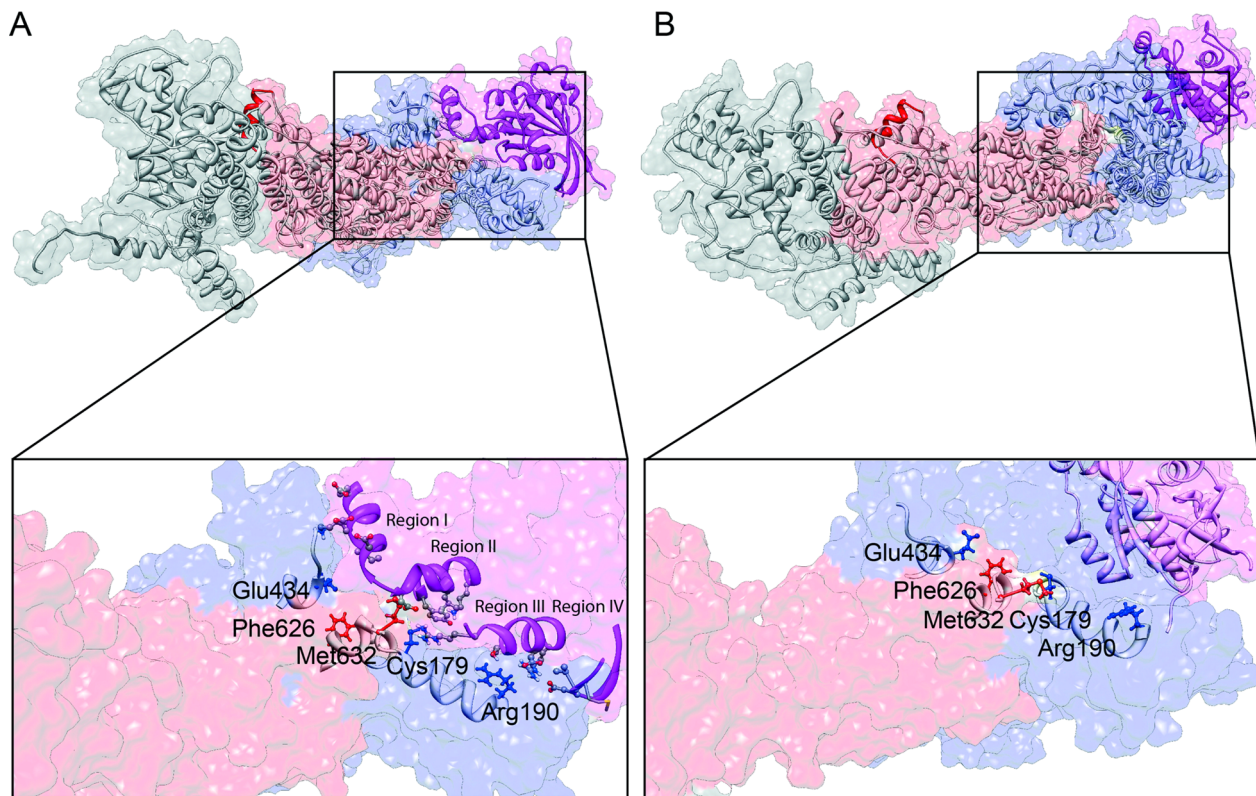


Figure 6. Interaction of CYFIP1 with RAC1 as characterized by analysis of the docking of RAC1 to (A) CYFIP1_{MD} and (B) CYFIP1_{XRAY}. In each panel, the zooming rectangle shows the RAC1-binding site on CYFIP1 that is enlarged in the detailed view below. RAC1 is shown in violet, while the main chain of CYFIP1 and relevant residues are shown in blue (N-terminal domain), red (central domain), and gray (C-terminal domain).

WRC crystal¹⁰ to a more globular one in which the two ends of the structure are bent toward each other. This novel structure explains the fact that the CYFIP1–eIF4E and CYFIP1–WRC complexes are mutually exclusive:⁷ while the eIF4E-binding site around helix H8b is partially buried in the central domain of CYFIP1 and covered by NCKAP1, the butterfly-like motion exposes it to the solvent. In addition, helix H8b reorients with respect to the central domain in a manner that optimizes the interaction surface for eIF4E. Accordingly, our docking study shows good binding affinity of eIF4E to the globular CYFIP1 structure (Figure 5), whose geometry is similar to those of complexes of eIF4E with other 4E-binding proteins (Figure S5 in the Supporting Information). Similar binding cannot be obtained with the CYFIP1 structure found in the WRC crystal. NCKAP1, a principal component of the WRC, instead contacts CYFIP1 over the entire side that is formed by the central and C-terminal domains.¹⁰ A bending of the two domains with respect to each other, as observed in the butterfly-like motion, is thus not compatible with NCKAP1 binding.

Starting from our previous finding that CYFIP1 exists in two conformations,⁷ here we have defined the dynamic landscape of the CYFIP1 conformational changes, describing for the first time its structural–dynamical determinant. The release of CYFIP1 from the WRC and its evolution in time (as simulated when free in solution) is accompanied by a concerted motion of the domains that reorganizes the entire structure and leads to a new stable conformation. We have defined at atomic resolution the rearrangements of the regions involved in the binding with eIF4E or Rac1 that occur during this motion.

Importantly, these findings complement previous experimental evidence from fluorescence resonance energy transfer

(FRET) measurements. In the WRC crystal, the N- and C-termini are 12 nm apart, and they do not come significantly closer during our simulation of the CYFIP1–NCKAP1 dimer. This distance is too long for a FRET signal. Still, fluorescent protein domains attached to the extreme termini of CYFIP1 show a FRET interaction,⁷ indicating that they are less than 10 nm from each other. Indeed, we found a distance of ~7 nm in the globular conformation (Figure 3). Moreover, the FRET distance decreases under conditions where the eIF4E–CYFIP1 complex is favored.⁷ This can best be explained by two CYFIP1 populations: one in the planar conformation that does not give a FRET signal and one in the globular conformation that shows a robust FRET interaction. The actual FRET signal measures the weighted average of the two populations and can change when CYFIP1 shifts from one conformation to the other.

The partitioning of CYFIP1 between the two conformations and hence between the different complexes is driven by synaptic stimulation, e.g., TrkB receptor signaling; RAC1 activation is required for the switch.⁷ Recently, additional biological evidence has been reported to support the notion that neuronal signaling shifts CYFIP1 between the two complexes.^{25,39,40} Our structural model makes a precise prediction of how RAC1–GTP might drive the switch: it binds strongly to the planar conformation but much less strongly to the globular conformation (Figure 6). Either weak binding of RAC1–GTP to the globular conformation changes the conformation of CYFIP1 in the manner of an induced fit or it binds and locks the planar conformation, thereby shifting the equilibrium. In both cases, CYFIP1 mutants defective in RAC1 binding¹⁰ should shift more to the globular conformation, even if globular CYFIP1 cannot integrate into the eIF4E complex. In

addition, RAC1–GTP would favor the disassembly of the translation inhibitory complex and at the same time provide more CYFIP1 for the formation of new WRCs. In the absence of active RAC1, an equilibrium will form between the two CYFIP1 conformations, i.e., CYFIP1 will take part in mRNA-silencing complexes and in inactive WRCs that await activation by RAC1–GTP.

A further factor to shift the equilibrium of CYFIP1 could be the vicinity to cell membranes: many membrane proteins exhibit WIRS peptides in their cytosolic domain that bind into the CYFIP1–NCKAP1 cleft and facilitate RAC1 binding.¹³ Vicinity to a suitable membrane increases the local concentration of these peptides, thereby augmenting the effect of RAC1–GTP and shifting the equilibrium away from the translation control complex. This model predicts that in the vicinity of a membrane enriched in WIRS peptides, local protein translation should be higher, in addition to increased actin dynamics.

While previous work^{7,25,39,40} showed that switching of CYFIP1 between the two complexes is relevant for the correct structure and function of neuronal synapses, here we have shown at the atomic level how the switch occurs. Our study therefore represents an excellent example of a multidisciplinary approach applied to clarify complex biological processes regulating brain function/s.

ASSOCIATED CONTENT

Supporting Information

Figures S1–S6 and a movie (AVI) showing the projection of the MD motions along the first eigenvector from the PCA analysis. The Supporting Information is available free of charge on the ACS Publications website at DOI: 10.1021/ct500431h.

AUTHOR INFORMATION

Corresponding Authors

*E-mail: claudia.bagni@cme.vib-kuleuven.be.

*E-mail: tilmann.achsel@cme.vib-kuleuven.be.

Present Addresses

○D.D.M.: Università della Svizzera Italiana (USI), Faculty of Informatics, Institute of Computational Science, Lugano, Switzerland.

◆S.D.R.: Seaver Autism Center for Research and Treatment, Department of Psychiatry, Icahn School of Medicine at Mount Sinai, New York, NY 10029, USA.

Author Contributions

The manuscript was written through contributions of all authors. All authors have given approval to the final version of the manuscript.

Funding

This work was supported by the Queen Elisabeth Foundation (FMRE-GSKE) Belgium, VIB, Associazione Italiana Sindrome X Fragile, and Compagnia San Paolo. D.D.M. and S.D.R. were supported by a Fonds Wetenschappelijk Onderzoek Grant (FWO G.0705.11) to C.B.

Notes

The authors declare no competing financial interest.

ACKNOWLEDGMENTS

The authors acknowledge the CASPUR Supercomputing Consortium for computational resources.

ABBREVIATIONS

CYFIP1, cytoplasmic FMRP interacting protein 1; Sra1, specifically RAC1 associated protein 1; FMRP, fragile X mental retardation protein; WRC, WAVE regulatory complex; MD, molecular dynamics; FRET, fluorescence resonance energy transfer; 4E-BP, eIF4E binding proteins; PCA, principal component analysis; SASA, solvent-accessible surface area; RMSF, root-mean-square fluctuation; RMSD, root-mean-square deviation; NCKAP1, NCK-associated protein 1

REFERENCES

- Jacquemont, S.; Hagerman, R. J.; Hagerman, P. J.; Leehey, M. A. Fragile-X syndrome and fragile X-associated tremor/ataxia syndrome: two faces of FMR1. *Lancet Neurol.* **2007**, *6*, 45–55.
- Bagni, C.; Tassone, F.; Neri, G.; Hagerman, R. Fragile X syndrome: causes, diagnosis, mechanisms, and therapeutics. *J. Clin. Invest.* **2012**, *122*, 4314–4322.
- Bassell, G. J.; Warren, S. T. Fragile X syndrome: loss of local mRNA regulation alters synaptic development and function. *Neuron* **2008**, *60*, 201–214.
- Zalfa, F.; Giorgi, M.; Primerano, B.; Moro, A.; Di Penta, A.; Reis, S.; Oostra, B.; Bagni, C. The fragile X syndrome protein FMRP associates with BC1 RNA and regulates the translation of specific mRNAs at synapses. *Cell* **2003**, *112*, 317–327.
- Schenck, A.; Bardoni, B.; Moro, A.; Bagni, C.; Mandel, J. L. A highly conserved protein family interacting with the fragile X mental retardation protein (FMRP) and displaying selective interactions with FMRP-related proteins FXR1P and FXR2P. *Proc. Natl. Acad. Sci. U.S.A.* **2001**, *98*, 8844–8849.
- Napoli, I.; Mercaldo, V.; Boyl, P.; Eleuteri, B.; Zalfa, F.; De Rubeis, S.; Di Marino, D.; Mohr, E.; Massimi, M.; Falconi, M.; Witke, W.; Costa-Mattioli, M.; Sonenberg, N.; Achsel, T.; Bagni, C. The fragile X syndrome protein represses activity-dependent translation through CYFIP1, a new 4E-BP. *Cell* **2008**, *134*, 1042–1054.
- De Rubeis, S.; Pasciuto, E.; Li, K. W.; Fernández, E.; Di Marino, D.; Buzzi, A.; Ostroff, L. E.; Klann, E.; Zwartkruis, F. J.; Komiyama, N. H.; Grant, S. G.; Poujol, C.; Choquet, D.; Achsel, T.; Posthuma, D.; Smit, A. B.; Bagni, C. CYFIP1 coordinates mRNA translation and cytoskeleton remodeling to ensure proper dendritic spine formation. *Neuron* **2013**, *79*, 1169–1182.
- Eden, S.; Rohatgi, R.; Podtelejnikov, A. V.; Mann, M.; Kirschner, M. W. Mechanism of regulation of WAVE1-induced actin nucleation by Rac1 and Nck. *Nature* **2002**, *418*, 790–793.
- Stradal, T. E.; Rottner, K.; Disanza, A.; Confalonieri, S.; Innocenti, M.; Scita, G. Regulation of actin dynamics by WASP and WAVE family proteins. *Trends Cell Biol.* **2004**, *14*, 303–311.
- Chen, Z.; Borek, D.; Padrick, S. B.; Gomez, T. S.; Metlagel, Z.; Ismail, A. M.; Umetani, J.; Billadeau, D. D.; Otwinowski, Z.; Rosen, M. K. Structure and control of the actin regulatory WAVE complex. *Nature* **2010**, *468*, 533–538.
- Schenck, A.; Bardoni, B.; Langmann, C.; Harden, N.; Mandel, J. L.; Giangrande, A. CYFIP/Sra-1 controls neuronal connectivity in *Drosophila* and links the Rac1 GTPase pathway to the fragile X protein. *Neuron* **2003**, *38*, 887–898.
- Kobayashi, K.; Kuroda, S.; Fukata, M.; Nakamura, T.; Nagase, T.; Nomura, N.; Matsuura, Y.; Yoshida-Kubomura, N.; Iwamatsu, A.; Kaibuchi, K. p140Sra-1 (specifically Rac1-associated protein) is a novel specific target for Rac1 small GTPase. *J. Biol. Chem.* **1998**, *273*, 291–295.
- Chia, P. H.; Chen, B.; Li, P.; Rosen, M. K.; Shen, K. Local F-Actin Network Links Synapse Formation and Axon Branching. *Cell* **2014**, *156*, 208–220.
- Ismail, A. M.; Padrick, S. B.; Chen, B.; Umetani, J.; Rosen, M. K. The WAVE regulatory complex is inhibited. *Nat. Struct. Mol. Biol.* **2009**, *16*, 561–563.
- Kim, Y.; Sung, J. Y.; Ceglia, I.; Lee, K. W.; Ahn, J. H.; Halford, J. M.; Kim, A. M.; Kwak, S. P.; Park, J. B.; Ryu, S. H.; Schenck, A.;

- Bardoni, B.; Scott, J. D.; Nairn, A. C.; Greengard, P. Phosphorylation of WAVE1 regulates actin polymerization and dendritic spine morphology. *Nature* **2006**, *442*, 814–817.
- (16) Lebensohn, A. M.; Kirschner, M. W. Activation of the WAVE complex by coincident signals controls actin assembly. *Mol. Cell* **2009**, *36*, 512–524.
- (17) Guex, N.; Peitsch, M. C. SWISS-MODEL and the Swiss-PDB Viewer: an environment for comparative protein modeling. *Electrophoresis* **1997**, *18*, 2714–2723.
- (18) Powell, M. J. D. An efficient method for finding the minimum of a function of several variables without calculating derivatives. *Comput. J.* **1964**, *7*, 155–162.
- (19) Phillips, J. C.; Braun, R.; Wang, W.; Gumbart, J.; Tajkhorshid, E.; Villa, E.; Chipot, C.; Skeel, R. D.; Kale, L.; Schulten, K. Scalable molecular dynamics with NAMD. *J. Comput. Chem.* **2005**, *26*, 1781–1802.
- (20) MacKerell, A. D., Jr.; Bashford, D.; Bellott, M.; Dunbrack, R. L., Jr.; Evanseck, J. D.; Field, M. J.; Fischer, S.; Gao, J.; Guo, H.; Ha, S.; Joseph-McCarthy, D.; Kuchnir, L.; Kuczera, K.; Lau, F. T. K.; Mattos, C.; Michnick, S.; Ngo, T.; Nguyen, D. T.; Prodhom, B.; Reiher, W. E., III; Roux, B.; Schlenkrich, M.; Smith, J. C.; Stote, R.; Straub, J.; Watanabe, M.; Wiórkiwicz-Kuczera, J.; Yin, D.; Karplus, M. All-Atom Empirical Potential for Molecular Modeling and Dynamics Studies of Proteins. *J. Phys. Chem. B* **1998**, *102*, 3586–3616.
- (21) MacKerell, A. D., Jr.; Feig, M.; Brooks, C. L. Extending the treatment of backbone energetics in protein force fields: limitations of gas-phase quantum mechanics in reproducing protein conformational distributions in molecular dynamics simulations. *J. Comput. Chem.* **2004**, *25*, 1400–1415.
- (22) Hess, B.; Bekker, H.; Berendsen, H.; Fraaije, J. LINCS: a linear constraint solver for molecular simulations. *J. Comput. Chem.* **1997**, *18*, 1463–1472.
- (23) Cheatham, T. E., III; Miller, J. L.; Fox, T.; Darden, T. A.; Kollman, P. A. Molecular Dynamics Simulations on Solvated Biomolecular Systems: The Particle Mesh Ewald Method Leads to Stable Trajectories of DNA, RNA, and Proteins. *J. Am. Chem. Soc.* **1995**, *117*, 4193–4194.
- (24) Darden, T.; York, D.; Pedersen, L. Particle mesh Ewald: an $N \cdot \log(N)$ method for Ewald sums in large systems. *J. Chem. Phys.* **1993**, *98*, 10089–10092.
- (25) Pathania, M.; Davenport, E. C.; Muir, J.; Sheehan, D. F.; López-Doménech, G.; Kittler, J. T. The autism and schizophrenia associated gene CYFIP1 is critical for the maintenance of dendritic complexity and the stabilization of mature spines. *Transl. Psychiatry* **2014**, *4*, No. e374.
- (26) Hoover, W. G. Canonical dynamics: equilibrium phase-space distributions. *Phys. Rev. A* **1985**, *31*, 1695–1697.
- (27) Nosé, S. A unified formulation of the constant temperature molecular dynamics methods. *J. Chem. Phys.* **1984**, *81*, 511–519.
- (28) Hess, B.; Kutzner, C.; van der Spoel, D.; Lindahl, E. GROMACS 4: Algorithms for Highly Efficient, Load-Balanced, and Scalable Molecular Simulation. *J. Chem. Theory Comput.* **2008**, *4*, 435–447.
- (29) *The PyMOL Molecular Graphics System*, version 1.2r2; Schrödinger, LLC: New York.
- (30) Pettersen, E. F.; Goddard, T. D.; Huang, C. C.; Couch, G. S.; Greenblatt, D. M.; Meng, E. C.; Ferrin, T. E. UCSF Chimera—a visualization system for exploratory research and analysis. *J. Comput. Chem.* **2004**, *25*, 1605–1612.
- (31) Amadei, A.; Linssen, A. B.; Berendsen, H. J. Essential dynamics of proteins. *Proteins* **1993**, *17*, 412–425.
- (32) Garcia, A. E. Large-amplitude nonlinear motions in proteins. *Phys. Rev. Lett.* **1992**, *68*, 2696–2699.
- (33) Daura, X.; van Gunsteren, W. F.; Mark, A. E. Folding–unfolding thermodynamics of a β -heptapeptide from equilibrium simulations. *Proteins* **1999**, *34*, 269–280.
- (34) Tomoo, K.; Matsushita, Y.; Fujisaki, H.; Abiko, F.; Shen, X.; Taniguchi, T.; Miyagawa, H.; Kitamura, K.; Miura, K.; Ishida, T. Structural basis for mRNA cap-binding regulation of eukaryotic initiation factor 4E by 4E-binding protein, studied by spectroscopic, X-ray crystal structural, and molecular dynamics simulation methods. *Biochim. Biophys. Acta* **2005**, *1753*, 191–208.
- (35) Tina, K. G.; Bhadra, R.; Srinivasan, N. PIC: Protein Interactions Calculator. *Nucleic Acids Res.* **2007**, *35*, W473–W476.
- (36) Mader, S.; Lee, H.; Pause, A.; Sonenberg, N. The translation initiation factor eIF-4E binds to a common motif shared by the translation factor eIF-4 gamma and the translational repressors 4E-binding proteins. *Mol. Cell. Biol.* **1995**, *15*, 4990–4997.
- (37) Hirshberg, M.; Stockley, R. W.; Dodson, G.; Webb, M. R. The crystal structure of human rac1, a member of the rho-family complexed with a GTP analogue. *Nat. Struct. Biol.* **1997**, *4*, 147–152.
- (38) Copley, S. D. Moonlighting is mainstream: paradigm adjustment required. *Bioessays* **2012**, *34*, 578–588.
- (39) Panja, D.; Kenney, J. W.; D'Andrea, L.; Zalfa, F.; Vedeler, A.; Wibrand, K.; Fukunaga, R.; Bagni, C.; Proud, C. G.; Bramham, C. R. Two-stage translational control of dentate gyrus LTP consolidation is mediated by sustained BDNF-TrkB signaling to MNK. *Cell Rep.* **2014**, *9*, 1430–1445.
- (40) Genheden, M.; Kenney, J. W.; Johnston, H. E.; Manousopoulou, A.; Garbis, S. D.; Proud, C. G. BDNF Stimulation of Protein Synthesis in Cortical Neurons Requires the MAP Kinase-Interacting Kinase MNK1. *J. Neurosci.* **2015**, *35*, 972–984.
- (41) Ceriotti, M.; Bussi, G.; Parrinello, M. Langevin equation with colored noise for constant-temperature molecular dynamics simulations. *Phys. Rev. Lett.* **2009**, *102*, 20601–20604.